Alliages à distribution bimodale de taille de grain : description numérique et analyses comparatives expérience-modélisation

Baptiste Flipon, Clément Keller, Fabrice Barbe

Bimodal grain-size distribution alloys: numerical description and experiments-simulations comparative analyses

B. FLIPON[a], C. KELLER[b], F. BARBE[c]

Normandie Univ, INSA Rouen, UNIROUEN, CNRS, GPM, 76000 Rouen, France

a. baptiste.flipon@insa-rouen.fr

b. clement.keller@insa-rouen.fr

c. fabrice.barbe@insa-rouen.fr

Résumé :

L'élaboration de nouveaux alliages métalliques à distribution bimodale de taille de grains ainsi qu'une compréhension fine des mécanismes de déformation de ces derniers sont à l'étude dans ces travaux. Ces alliages présentent deux populations de taille de grains distinctes : une à gros grains qui contribue à la ductilité et une à grains ultrafins qui améliore la limite d'élasticité et la contrainte à rupture du matériau. Alors que la plupart des propriétés mécaniques effectives (macroscopiques) de ces matériaux peuvent être obtenues à partir d'essais de traction, l'étude et la compréhension des mécanismes microstructuraux mis en jeu au cours de la déformation du matériau demandent un travail de préparation et d'analyse et/ou des moyens conséquents. L'utilisation de microstructures virtuelles et de la plasticité cristalline peut, en complément d'analyses microstructurales expérimentales, permettre une autre approche pour l'analyse des champs locaux de contrainte et déformation.

Abstract :

The elaboration of new metallic alloys with bimodal grain size distribution and accurate understanding of their deformation mechanisms are under study in this work. These alloys are composed of two distinct grain size populations: a coarse grain one which promotes material ductility and an ultrafine grain one which improves material yield stress and ultimate tensile strength. While effective (macroscopic) mechanical properties can be obtain from standard tensile tests, the study and understanding of microstructural deformation mechanisms require time-consuming and/or high-level experimental analysis technics. By using virtual microstructures and crystal plasticity, it is possible, in addition with experimental observations, to study local strain and stress fields.

Keywords : bimodal alloys, 316L, crystal plasticity, microstructural analyses, finite element analyses

1 Introduction

As opposed to the development of new austenitic stainless steel alloys based on the control of the chemical composition, recently new elaboration means have been proposed and studied. By tayloring the

microstructure and particularly by acting on Grain-Size (GS) reduction [1–3] and GS distribution [4] it is possible to elaborate ductile metallic alloys with high yield stress (resp. ultimate tensile strength). Bimodal GS distribution alloys (*i.e.* alloys with a GS contrast between two GS populations) with ductile Coarse Grains (CG) and high mechanical strength UltraFine Grains (UFG) can be obtained by two elaboration routes which have been adopted in this study. The first one is based on Powder Metallurgy (PM) and Spark Plasma Sintering (SPS) which enable a good control of GS populations but a limited GS contrast between CG and UFG [4–6]. The second is based on plasticity induced martensite and a reversion-annealing process: 316L austenitic samples are Cold-Rolled (CR) and then Heat Treated (HT). Using a well defined heat treatment one can observe UFG at the former martensite sites and CG on heavily strained and recrystallized austenite [5, 7]. Tensile tests on bimodal alloys obtained by both elaboration routes are then performed. Microstructural analyses are also realized in order to provide morphological and statistical inputs for numerical microstructure-based investigations. Polycrystalline bimodal aggregates are generated by means of controlled Laguerre-Voronoi tessellations through Neper software [8]. Full-field crystal plasticity Finite Element (FE) analyses are then performed using Zset software [9]. Two material constitutive laws are used: a Schmid-based phenomenological law [10] taking into account the GS effect by an empirical Hall-Petch type coefficient and a more physical law based on dislocation density evolution [11]. The phenomenological law, due to its low computation cost, enables analyses on large and representative polycrystalline aggregates whereas the physics-based law provides more physically accurate local strain and stress fields. Complementary analyses between the first experimental and numerical results are finally provided and discussed.

2 Experimental elaboration routes: description and microstructural analyses

As previously stated in introduction, PM+SPS route enables to control the GS populations in bimodal alloys. This elaboration process is indeed based on blends of different GS powders and by controlling powders volumic fraction and/or by using different ball-milling conditions one can elaborate a large range of bimodal alloys [4]. Moreover, after sintering, the material texture is low and grains are mostly equiaxed: these conditions are favorable for a precise study of the effect of bimodality on the mechanical response of the material. However this route can be time-consuming (due to ball-milling steps) and can only provide samples with limited dimensions (50 mm diameter and 5-6 mm height cylinder).

On the other side, martensite reversion-annealing process is easier to execute and larger tensile test specimens can be obtained. Nevertheless, the control of GS populations in terms of spatial and size distribution is not as precise as with PM+SPS route.

Figure 1 presents two bimodal samples obtained by both aforementioned process routes. One can note that PM+SPS route tends to provide a more regular spatial distribution of CG and a limited CG clustering whereas CR+HT process leads to localized CG clusters. The contrast between the GS populations obtained in these two cases is also different: the ratio CG size over UFG size in the SPS case is around 5 (UFG 500 nm and CG 2.5 μm) while in the CR+HT case this ratio is closer to 10 (UFG 1 μm and CG 10 μm).

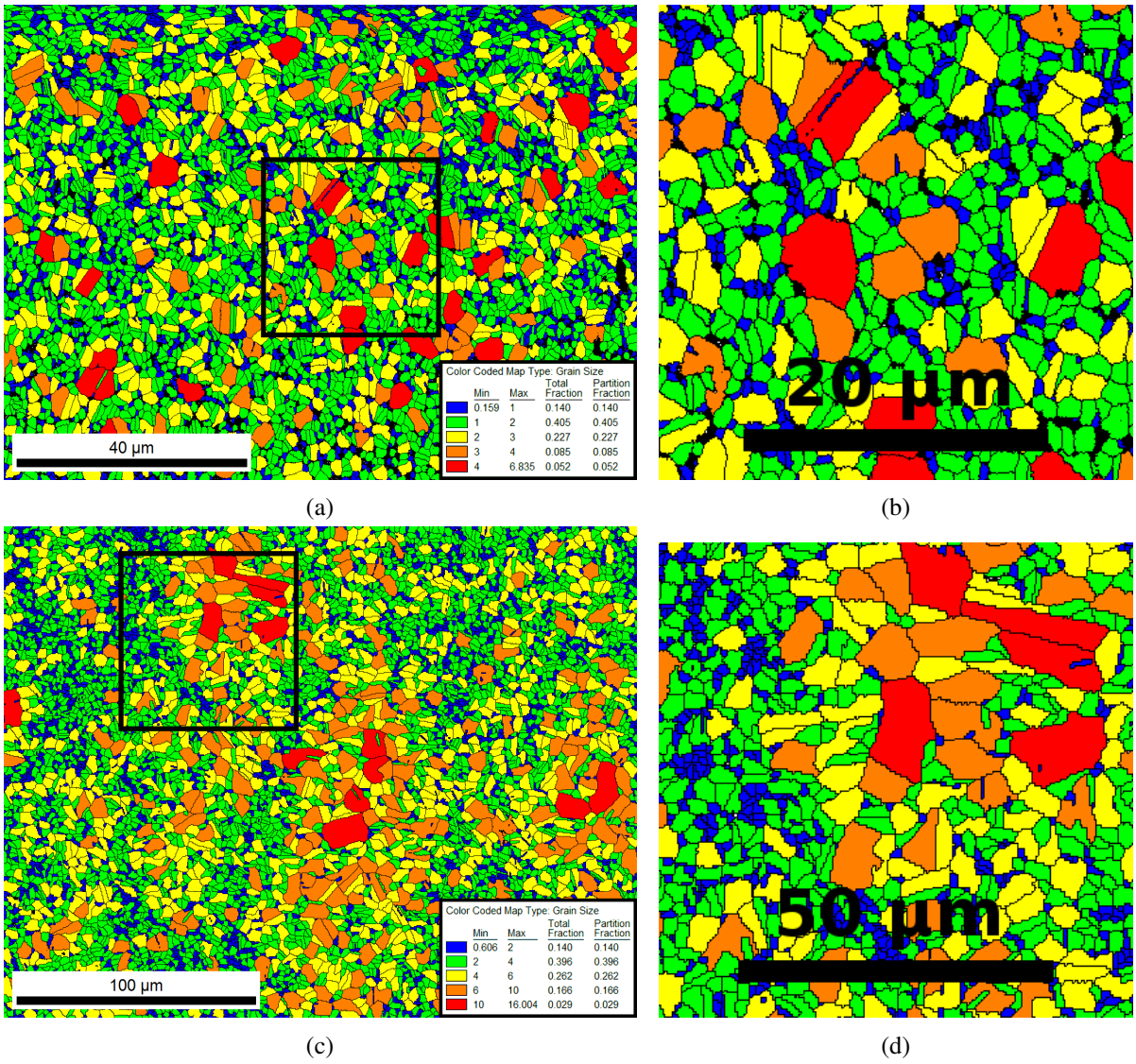

Figure 1 – (a) and (c) EBSD color maps based on grain-size for (a) a 50% CG - 50% UFG (volume fractions) blend of powder sintered by SPS and (c) a cold-rolled (up to 71% thickness reduction) sample and heat-treated at 850°c during 20 minutes. (b) and (d) provide zooms on the zones highlighted in (a) and (c).

3 Numerical description: microstructure generation, crystal plasticity law and computed stress and strain fields

Microstructures are obtained from the combination of a controlled nuclei generation with a Laguerre-Voronoi tessellation. This process is described in Figure 2 on a simple case with a single coarse grain. By using this pre-processing and options available in Neper software [8] one can generate more complex representative microstructures close to experimental ones (Figure 4(b) and (f)). Tessellations are then meshed in order to perform crystal plasticity finite element analyses. In this paper a focus is made on results obtained with the phenomenological law (small strains formulation). Constitutive equations (1-2) describe the phenomenological law [10] with modified isotropic hardening to take into account GS effect.

$$\dot{\gamma}^s = \left\langle \frac{|\tau^s - x^s| - r_g^s}{K} \right\rangle^n \text{sign}(\tau^s - x^s) \qquad x^s = 0 \tag{1}$$

$$r_g^s = r_{0\,g} + Q \sum_{u=1}^{12} h^{su} \left(1 - e^{-bp^u}\right) + \frac{k_g}{\sqrt{d_g}} \tag{2}$$

Resolved shear stress (τ^s), isotropic (r^s) and cinematic (x^s) hardening terms are used to describe the plastic flow rate ($\dot{\gamma}^s$) on the considered slip system s. Plastic flow occurs on the system s when resolved shear stress τ^s reaches a critical value τ_c^s. K and n describe the Norton viscosity. Kinematic hardening is not considered here and then $x^s = 0$. The isotropic hardening r_g^s is computed for each slip system s and for each grain g in order to take into account the GS distribution in the aggregate. h^{su} matrix describes slip systems interactions. Q and b are classical terms for non-linear hardening which respectively act on the saturation value and the hardening of the law. $r_{0\,g}$ and the Hall-Petch term $\frac{k_g}{\sqrt{d_g}}$ describe the onset of plasticity in each grain. Extended description of the initial model can be found in [10].

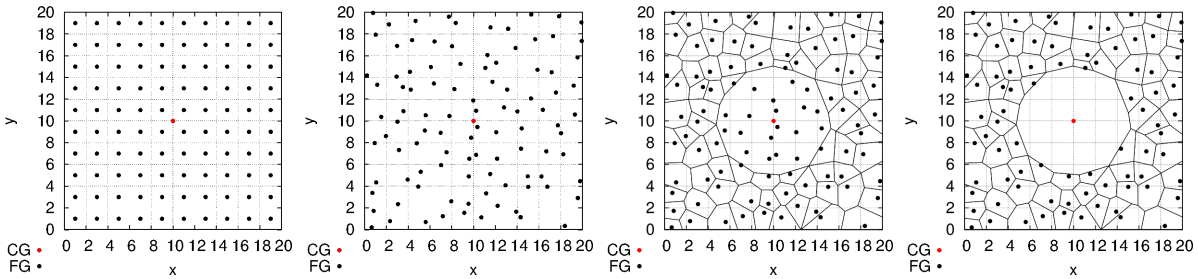

Figure 2 – Tessellation generation process: (a) initial seeds position, (b) seeds are randomly perturbated within a given region around initial positions, (c) and (d) seeds surrounding the CG are suppressed and subdivision is processed according to the weights assigned to each nucleus.

4 Analyses on an experimental and numerical ground

Figure 3 provides the tensile stress-strain curves for first experimental tests and numerical microstructure presented in Figure 4(b)(f). Numerical effective responses (*i.e.* axial strain and stress averaged over all the elements) are close to those of the experimental sample obtained by SPS with an unimodal ($d_{mean} = 3\mu m$) GS distribution. This can be explained by the low contrast in GS observed in the current numerical microstructure: since $d^{UFG} \simeq 2\mu m$ and $d^{CG} \simeq 5\mu m$ the expected hardening effect from the UFG population is limited. The hardening coefficient is lower in the case of numerical computations than for experimental results: material law parameters might be re-identified on bimodal experimental curves to improve hardening modelling. Regarding bimodal experimental curves one can note that for the one obtained by CR+HT the yield stress is two times higher than in the other cases. Extensive Scanning Electron Microscopy observations have shown residual heavily strained austenite grains which did not recrystallize during HT. Work is currently under progress to obtain CR+HT samples with totally recrystallized residual austenite, thus enabling to characterize only bimodal GS distribution effect on effective mechanical properties.

Nevertheless and even if GS scaling between experimental and numerical microstructures is not accurate, Figures 4(c)-(d)-(g)-(h) provide information on strain and stress localization. One can, in particular,

note that CG clusters (Fig. 4(c) and (g)) tend to favor strain localization whereas stress are more homogeneously distributed in the UFG matrix (Fig. 4(d) and (h)).

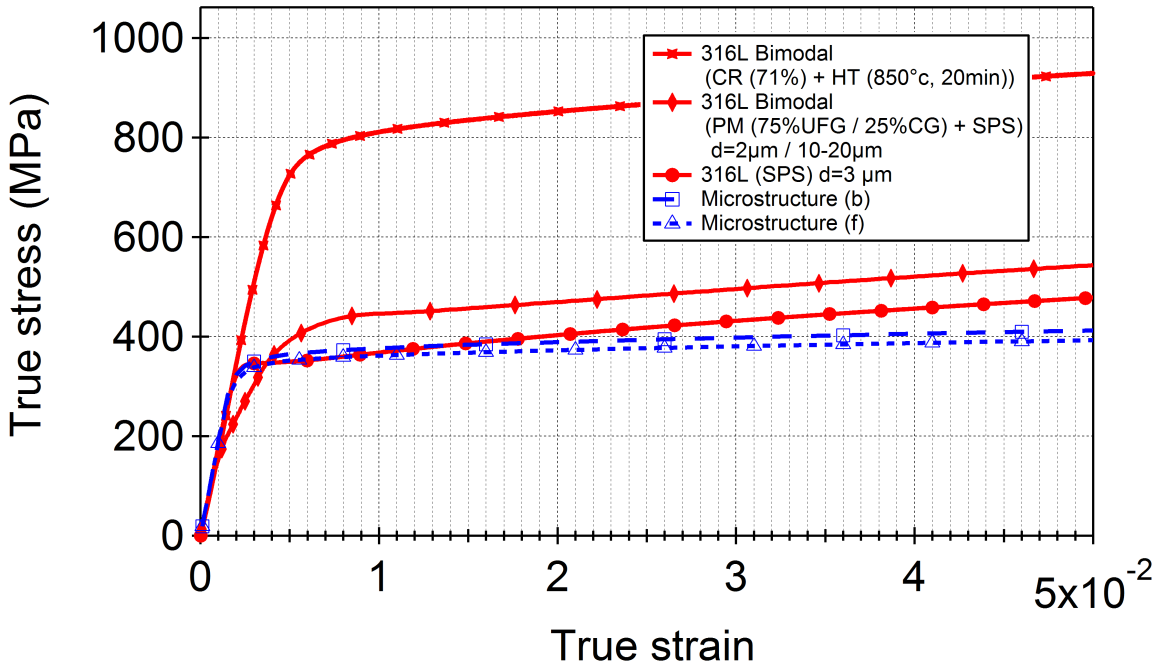

Figure 3 – Computed (in blue) and experimental (in red) tensile curves for bimodal alloys employed in this study.

5 Conclusions

A coupled experience and modelling microstructure-based approach is currently being developped in order to characterize both macroscopic and local effects of a bimodal microstructure on the plasticity of a 316L alloys. Two elaboration routes have been explored to obtain a wide range of bimodal GS distributions: with different volumic fraction of CG and UFG populations and also different microstructure morphologies (CG clusters). Tensile tests have been performed and results have been analyzed with a focus on hardening and fracture mechanisms. These results and the related microstructural analyses constitute input data for microstructure numerical description and for the identification of crystal plasticity parameters. FE analyses provide valuable information about the role of the bimodal microstructure, not only from the standpoint of the volume fraction of each GS population but also regarding their spatial arrangement, *e.g.* the clustering degree of CG.

Complementary and extensive analyses are currently performed to enrich both experimental and numerical databases and results are soon to be expected.

Acknowledgements

Authors thank the Normandie region and the European Community for their financial support through the SUPERMEN project. Thanks are also due to R. Quey for providing highly valuable help in the use of Neper. L. Garcia de la Cruz and E. Hug (CRISMAT) are acknowledged for their help and experimental support concerning ball-milling and spark plasma sintering.

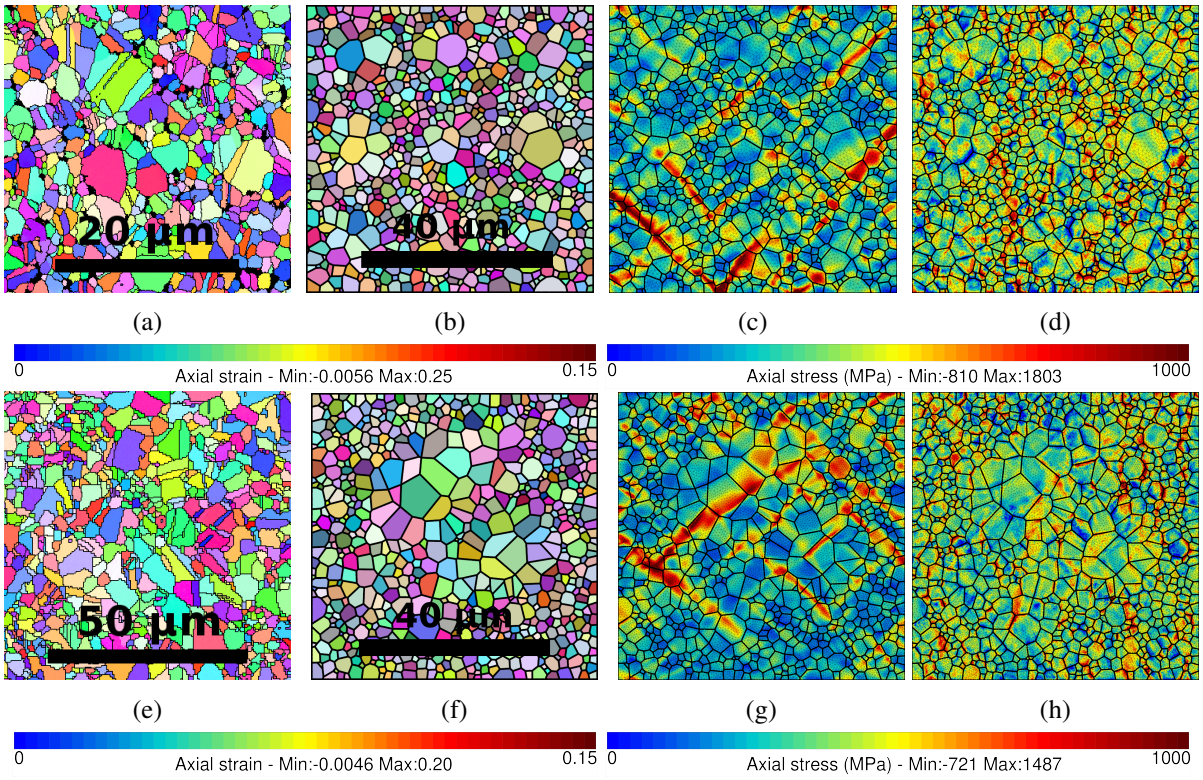

Figure 4 – (a) and (e): EBSD orientation maps of experimental samples obtained by (a) PM+SPS and (e) CR+HT. (b) and (f): numerical microstructures which can qualitatively be compared to the experimental ones. (c) and (g): strain fields (tension to 5%) on 2D-extruded microstructures (resp. (b) and (f)). (d) and (h) present the corresponding stress fields.

References

[1] E. O. Hall. The deformation and ageing of mild steel: III discussion of results. *Proceedings of the Physical Society. Section B*, 64(9):747–753, sep 1951.

[2] N. J. Petch. The cleavage strength of polycrystals. *Journal of Iron and Steel Institute*, 173:25–27, 1953.

[3] H. Gleiter. Nanocrystalline materials. *Progress in Materials Science*, 33(4):223–315, 1989.

[4] Z. Zhang, S. K. Vajpai, D. Orlov, and K. Ameyama. Improvement of mechanical properties in SUS304l steel through the control of bimodal microstructure characteristics. *Materials Science and Engineering: A*, 598:106–113, mar 2014.

[5] B. Flipon, F. Barbe, C. Keller, and R. Quey. Influence of bimodal microstructure on mechanical properties : a full-field crystal plasticity approach. Eur. Mech. Mater. Conf. 15, Brussels, September 7-9th, 2016, 2016.

[6] G. Dirras, J. Gubicza, S. Ramtani, Q.H. Bui, and T. Szilágyi. Microstructure and mechanical characteristics of bulk polycrystalline ni consolidated from blends of powders with different particle size. *Materials Science and Engineering: A*, 527(4-5):1206–1214, feb 2010.

[7] S. Sabooni, F. Karimzadeh, M.H. Enayati, and A.H.W. Ngan. The role of martensitic transforma-

tion on bimodal grain structure in ultrafine grained AISI 304l stainless steel. *Materials Science and Engineering: A*, 636:221–230, jun 2015.

[8] R. Quey, P.R. Dawson, and F. Barbe. Large-scale 3d random polycrystals for the finite element method: Generation, meshing and remeshing. *Computer Methods in Applied Mechanics and Engineering*, 200(17-20):1729–1745, apr 2011.

[9] Zset. http://www.zset-software.com, 2012.

[10] L. Méric, P. Poubanne, and G. Cailletaud. Single crystal modeling for structural calculations: Part 1- model presentation. *Journal of Engineering Materials and Technology*, 113(1):162, 1991.

[11] L. Tabourot, M. Fivel, and E. Rauch. Generalised constitutive laws for f.c.c. single crystals. *Materials Science and Engineering: A*, 234-236:639–642, aug 1997.